applied sciences

MDPI

Article

The Impact of Automated Vehicles on Road and Intersection Capacity

Quan Yu *,†, Longsheng Wu †, Haonan Zhang *,†, Linlong Lei and Li Wang

School of Electrical and Control Engineering, North China University of Technology, Beijing 100144, China; m18505695170@163.com (L.W.); linlong@mail.ncut.edu.cn (L.L.)

* Correspondence: yuquan@ncut.edu.cn (Q.Y.); zhn17513632114@163.com (H.Z.)

† These authors contributed equally to this work and should be considered as co-first authors.

Abstract: With the rapid development of autonomous driving technology, future road traffic must be composed of autonomous vehicles and artificial vehicles. Although autonomous vehicles have greatly improved road capacity, few studies have involved capacity at signal-controlled intersections, and most of the studies are based on experimental simulation. As such, there is a need to more scientifically analyze the impact of autonomous vehicles on road and intersection capacity. Based on three theories of flow-density relationships, traffic flow equilibrium analysis, and the following model, this paper firstly deduces the flow-density relationship of different vehicle types in a single environment. Secondly, flow-density relationships under different proportions of self-driving vehicles are derived. Through the derivation of these two models, the basic road saturation flow rates under different permeabilities of self-driving vehicles, can be obtained. Based on these results, a revised calculation model for the capacity of signalized intersections with different proportions of autonomous vehicles is proposed, which is essentially to revise the basic saturation flow rate under different permeabilities of autonomous vehicles. By using SUMO 1.15.0 traffic simulation software, the theoretical models are individually tested. The results show that the error rate between the theoretical calculation results and the SUMO simulation results, is less than 16%. This study can provide a basis for the calculation of basic capacity of roads and intersections in a future man-machine hybrid driving environment, and provide theoretical guidance for traffic management and control.

Keywords: autonomous vehicle (AV); capacity; man-machine hybrid driving environment; traffic flow basic map model; following model; SUMO

Citation: Yu, Q.; Wu, L.; Zhang, H.; Lei, L.; Wang, L. The Impact of Automated Vehicles on Road and Intersection Capacity. *Appl. Sci.* **2023**, *13*, 5073. https://doi.org/10.3390/app13085073

Academic Editor: Ke Gu

Received: 22 March 2023
Revised: 10 April 2023
Accepted: 11 April 2023
Published: 18 April 2023

1. Introduction

With the rapid development of technology and economy in modern society, and the continuous improvement of vehicle automation, autonomous vehicles are expected to be gradually promoted and applied in people's productions and lives from the theoretical level. It can be predicted that the vehicle composition of urban traffic in the future will inevitably be a mixture of human-driven vehicles and autonomous vehicles [1]. Various problems faced by urban traffic in the past, such as traffic safety and road congestion, are expected to be solved with the help of various advantages of autonomous vehicles. Therefore, it is necessary to study the impact of autonomous vehicles on road and intersection capacity.

For a long time, scholars have divided the impact of autonomous vehicles on traffic into two aspects: one is the study of road capacity; the other is the study of traffic flow stability. Research on road capacity can greatly alleviate traffic congestion and improve residents' driving experiences, so there are many achievements in recent years.

Park et al. studied the impact of autonomous vehicles on urban road capacity through a microsimulation method. VISSIM 2020 simulation software was used to build a road network, and parameters of the Wiedmann 74 following model were changed, in order to simulate human-driven vehicles and autonomous vehicles, respectively. The study found

that increased AV penetration will improve traffic flow, reduce average vehicle delays, and increase road capacity by 40% when AV penetration reaches 100% [2]. Similarly, Beza et al. studied the impact of autonomous automated vehicles (AAVs) and cooperative automated vehicles (CAVs) on highway traffic capacity, through VISSIM simulation software. The results show that CAV has a stronger impact on improvement of traffic capacity, regardless of highway section type [3]. Song et al. studied the impact of intelligent connected vehicles (ICVs) and traditional human-driven vehicles (HVs) on highway capacity in China, and the results showed that, although ICVs significantly improved capacity at high traffic inputs, at low and moderate traffic inputs, the benefits were not obvious [4]. Lu et al. investigated the effect of autonomous vehicles on the macroscopic fundamental diagram (MFD), and showed that as AV penetration increased, so too did the capacity of the road network [5]. Mavromatis et al. investigated and quantified vehicles in road networks in Europe and the United States, and proved, through numerical simulation experiments, that traffic congestion could be reduced by four times under the same traffic flow running speed [6]. Ghiasi et al. proposed a road capacity analysis model in a man-machine hybrid driving environment, by using the improved Markov chain. Through experimental verification, this model can accurately quantify the corresponding traffic capacity [7]. Van Arem et al. established the expressway as the research object, and found, through simulation experiments, that, for the transitional section with a reduced number of lanes, the traffic capacity of the section could be improved only when the proportion of CACC vehicles was higher than a specific value [8].

In addition, many studies have shown that AVs can improve road capacity [9–12]. However, some studies suggest that the improvement will not be significant until penetration of autonomous vehicles reaches a certain limit.

Werf et al. used the Monte Carlo method, that is, the statistical simulation method, to study the influence of autonomous vehicles on highway traffic capacity under two following models, and carried out sensitivity analyses of some parameters in ACC and CACC following models. The results show that the road capacity will reach 30% when the time headway of ACC is 1 s, but it will decrease when the time headway is 1.4 s [13]. Likewise, Jones and Philips have also noted in their paper that traffic flow can only be improved when the penetration rate of ACC or CACC autonomous vehicles on the road, reaches 40% [14]. Calvert et al. built a 19 km long 3-lane highway, and the experimental results showed that the traffic flow would be improved only when the penetration rate of self-driving vehicles exceeded 70%, and the traffic flow would decrease slightly when the penetration rate reached 80% [15]. Tientrakool et al. found that road capacity can be improved only when the penetration rate of CACC autonomous vehicles exceeds 85% [16].

For the existing research, the experimental means are obtained through simulation experiments, some from the macro level of the entire road network simulation, others from the micro level of a certain section of road simulation [17–22]. For autonomous vehicles, as they are still in the testing phase, simulation is still the main research method [23–25].

In order to more rigorously analyze the impact of AVs on road capacity, this paper deduces the improvement of road capacity by AVs in different proportions, based on three theories of traffic flow-density relationships, a vehicle-following model, and the traffic flow equilibrium state. Existing studies have not analyzed in detail, the impact of Avs on the capacity of signal-controlled intersections. Based on the analysis of road capacity, this paper further extends to intersections, to provide the corresponding basis for signal control in the future man-machine hybrid driving environment. The main research undertaken in this paper is as follows.

(1) Based on a basic traffic flow diagram model, traffic flow equilibrium analysis, and a vehicle-following model, a study of the flow-density relationship of homogeneous traffic flow on a single lane road, is proposed.
(2) Further, based on the proportional derivation of human-driven vehicles and two kinds of autonomous vehicles, the flow-density relationships of heterogeneous traffic flow

on single-lane roads, is obtained. These data are used to analyze the road capacities under different proportions of autonomous vehicles.

(3) Based on the traditional signalized intersection capacity calculation model, the revised calculation model of capacity in a mixed environment is obtained, the essence of which is to correct the basic saturated flow rate under different proportions of autonomous vehicles, in order to provide theoretical guidance for future signalized intersection control.

(4) Finally, SUMO simulation software was used, to verify the accuracy of the above three models.

The structure of this article is as follows. Section 2 introduces the theoretical research methods used in this paper. Section 3 studies the flow-density relationship of single lane road traffic flow in a single environment. Section 4 studies the flow-density relationship of single lane road traffic flow in a mixed environment. In Section 5, the capacity of signalized intersections under a man-machine hybrid driving environment is studied. Section 6 comprises the summary of the article, and the development of future work.

2. Methods

2.1. U.S. Highway Capacity Manual Method

There are many calculation methods of traffic capacity at home and abroad, and the principles of each are quite different. Among them, the most widely used is the U.S. HCM method [26–28].

For the calculation of capacity at signal-controlled intersections, the American HCM method is obtained by reducing the basic saturated flow rate. Basic saturated flow rate refers to the maximum road traffic flow at the entrance of an intersection, under the conditions of good weather, good road condition, traffic flow consisting only of cars, and good visual distance of drivers, generally using 1800 pcu/h. When using this method, the basic saturation flow rate is selected first. Then, it is reduced, in order to obtain the revised saturated flow rate of each lane, as shown in Formula (1). Then the traffic capacity of each lane is calculated using the green signal ratio, as shown in Formulas (2) and (3). Finally, the total capacity of signal-controlled intersections can be obtained by summing the capacity of each inlet lane.

$$S_i = S_0 \times N \times f_w \times f_{HV} \times f_g \times f_p \times f_{bb} \times f_a \times f_{LU} \times f_{LT} \times f_{RT} \times f_{Lpb} \times f_{Rpb}, \quad (1)$$

where S_i is the lane group i saturation flow rate, S_0 is the saturation flow rate of the lane group under ideal conditions (the basic saturation flow rate), N is the number of lanes in this lane group, f_w is the lane width correction factor, and f_{HV} is the heavy vehicle correction factor, which satisfies the following formula: $f_{HV} = \frac{1}{1+P_T(E_T-1)}$, where P_T is the proportion of heavy vehicles, E_T is the passenger car equivalent value of heavy vehicles, f_g is the approach slope correction factor, f_p is the parking in the adjacent lane and the correction factor for the number of stops in that lane (i.e., it illustrates the impact of parking on the nearby lanes and the occasional blocking effect of traffic access to the adjacent lanes), f_{bb} is the correction factor for the effect of obstruction within the intersection where the bus is parked (i.e., the impacts of having the bus stop located before the intersection and after the intersection are illustrated), f_a is the area type correction factor in the business district, and f_{LU} is the lane utilization correction factor (lane utilization correction mainly considers the uneven distribution of traffic volume in several lanes of a certain lane group with multiple lanes). The correction coefficient mainly considers the highest flow lane, where: f_{LT} is the lane group left turn correction factor, in situations where there is a special phase for left turns and a special lane; f_{RT} is the lane group right turn correction factor; special lane $f_{RT} = 0.85$; shared lane $f_{RT} = 1.0 - 0.5P_{RT}$; single lane $f_{RT} = 1.0 - 0.135P_{RT}$; P_{RT} is the right turn ratio; f_{Lpb} is the correction factor for left-turning pedestrians; and f_{Rpb} is the correction factor for right turns of pedestrians and bicycles.

$$C_i = S_i \lambda_i, \tag{2}$$

$$\lambda_i = \frac{g_i}{T}, \tag{3}$$

where C_i is the capacity of lane group i; λ_i is the green ratio of the lane group i (it refers to the proportional time that traffic lights can be used for vehicles to pass within a cycle, that is, the ratio of the effective green time of a certain phase, to the duration of the cycle); and g_i is the effective green time of lane group i, i.e., the effective green time of this phase is the time actually used for vehicle passing, after subtracting the total loss time of this phase from the sum of the actual green time and interval time displayed at a certain phase. The effective green time of a cycle is defined as the cycle time minus the total loss time within the cycle. T is the signal period length.

Before calculating the saturation flow rate, necessary data such as intersection geometry, traffic volume, and road traffic conditions, are required [29].

2.2. Analysis of Intersection Capacity

In order to calculate the traffic capacity of intersections in mixed environments and analyze the impacts made by autonomous vehicles in different proportions on signal-controlled intersections, it is necessary to obtain the basic saturation flow rate of the road, and then obtain the revised saturation flow rate, by converting the basic saturation flow rate, and finally calculate the traffic capacity.

In order to calculate the basic saturated flow rate of a road in a mixed environment, that is, the maximum traffic volume passing through a certain section of the road, it is necessary to rely on the flow-density relationships in the basic traffic flow diagram model, the following model of artificial and autonomous vehicles, and the equilibrium analysis of traffic flow.

2.3. Traffic Flow Basic Map Model

The basic diagram model of traffic flow describes the relationship among traffic volume, lane density, and vehicle speed, and is a basic model in traffic flow theory and traffic engineering. The basic traffic flow map model can be used to calculate the basic road capacity, and has a priori theoretical guiding significance for analyzing the impact of the permeability of autonomous vehicles on the capacity of roads and signalized intersections in the future man-machine mixed environment.

The density calculation formula is shown in (4). Road density reflects the number of vehicles in the lane and the degree of traffic congestion. The higher the density, the more crowded the section.

$$K = \frac{N}{L}, \tag{4}$$

where K representation density, N represents the number of vehicles on the road, and L represents the road length.

The relationship between the three parameters can be expressed by Formula (5).

$$Q = vK, \tag{5}$$

where Q is the traffic volume, v is the speed.

In 1934, Greenshields proposed the "speed-density" model in his paper [30], in which the "flow-density" model and the "flow-velocity" model could be obtained. These three models are the core of the basic diagram model of traffic flow. Among the relationships among flow, density, and speed, the relationship between flow and density is the most widely used, and it is also the main research object of this paper.

Using the three-parameter basic relationship of traffic flow (5), along with Greenshields' speed-density relationship (6), the flow-density relationship can be derived, as shown in Equation (7).

$$v = v_f(1 - \frac{K}{K_j}), \tag{6}$$

$$Q = Kv_f(1 - \frac{K}{K_j}) = v_f(K - \frac{K^2}{K_j}), \tag{7}$$

where v_f represents free travel speed, and K_j represents blocking density.

It can be seen from Equation (7) that the "flow-density" model used in the traditional manual driving environment, is a quadratic function.

2.4. Traffic Flow Equilibrium State Analysis

The equilibrium state of traffic flow refers to the ideal state, where the traffic density of a road remains constant, and all vehicles maintain the same speed. Through the analysis of the balanced state of the artificially driven vehicle, the flow-density relationship diagram can be obtained. Although the self-driving vehicle has not been driven on roads on a large scale at the present stage, we may assume that, under ideal conditions, the self-driving vehicle must eventually form a balanced state, that is, all vehicles have the same speed, zero speed difference, and zero acceleration. In the equilibrium state, since the road density is constant and the vehicle speed is the same, the time headway between vehicles must also be the same. With the help of the equilibrium "speed-headway" function relationship, the basic road capacity under different traffic environment can be deduced.

For traffic flow with the same vehicle composition in a single environment, all vehicles have the same speed and time headway when they reach the equilibrium state. For traffic flow with different vehicle compositions in mixed environments, when all vehicles reach the equilibrium state, the speed is the same, but the distance between the heads is different. The difference of the following model will result in different relationships between the balance speed and the distance between the heads of different vehicles.

Let h_{dI}, h_{dA}, and h_{dC} represent the equilibrium space headway of an artificial vehicle and an autonomous vehicle, respectively, where Formula (8) represents the relationship between the equilibrium speed and space headway.

$$\begin{cases} h_{dI} = f_I(v_b) \\ h_{dA} = f_A(v_b) \\ h_{dC} = f_C(v_b) \end{cases}, \tag{8}$$

where v_b represents equilibrium speed, and f_I, f_A, and f_C represent the "speed-front distance" function relationships of the balanced states of manual, ACC autonomous driving, and CACC autonomous driving vehicles, respectively.

2.5. Following Model and Parameter Calibration

2.5.1. The IDM Following Model

The intelligent driver model was proposed by Treiber in 2000 [31]. The specific model is shown in Formulas (9)–(11).

$$a_n(t) = a\left[1 - (\frac{v_n(t)}{v_0})^{\delta} - (\frac{s^*}{s_n(t)})^2\right], \tag{9}$$

$$s^* = s_0 + v_n(t)T + \frac{v_n(t)\Delta v}{2\sqrt{ab}}, \tag{10}$$

$$s_n(t) = h_n(t) - l, \tag{11}$$

where $a_n(t)$ represents the acceleration of the vehicle; $v_n(t)$ represents the speed of the vehicle; v_0 represents the (expected) speed of the vehicle in free flow; δ represents the vehicle acceleration index, whose value is generally 4; s^* represents the distance between the front bumper of the rear car and the rear bumper of the front car; $s_n(t)$ represents

the actual vehicle spacing at the time; s_0 represents the minimum expected (safe) vehicle spacing; T represents the expected (minimum) headway; Δv is the speed difference between the front and rear vehicles; a represents the maximum acceleration of vehicle in free flow; b represents the comfortable rate of deceleration or the desired rate of deceleration; $h_n(t)$ represents the distance between the front bumper of the rear car and the front bumper of the front car at the moment; and l represents the length of the vehicle.

Although the IDM following model lacks random items compared with other human-driven vehicle-following models, in view of its small number of parameters and clear significance, the IDM following model can naturally and continuously simulate vehicle following behavior under different traffic conditions in a concise form, which is in good agreement with a large amount of measured data. Therefore, it is used as a driving model for manual vehicles. Based on the statistical analysis of the vehicle data measured on the road, and the recommended value of the reference model, the model parameters are proposed as follows, as shown in Table 1.

Table 1. The IDM following model, where parameter specifies the value.

Parameter	Value
a	1
v_0	34
s_0	1.5
b	2
l	5
T	1.5

2.5.2. The ACC Following Model

At present, autonomous vehicles are mainly divided into two categories. The first category is autonomous vehicles based on adaptive cruise control [32]. By means of the vehicle's own sensors, such as the vehicle camera, microwave radar, millimeter-wave radar, etc., it can sense other vehicles, non-motor vehicles, pedestrians, and transportation infrastructure around the vehicle, and then calculate through the vehicle processor, and finally control the vehicle, to make it behave appropriately. It is also the research direction of many enterprises, both at home and abroad.

Since ACC autonomous vehicles are rarely, or even never, operated on a road in real road traffic, so research related to this driving model remains mostly theoretical. Parameters of traditional human-driven vehicle-following models (such as IDM, LCM, FVD, etc.), are changed, to simulate the man-machine mixed environment, and then the characteristics of heterogeneous traffic flow are studied. Since it is based on the following model of artificial vehicles, it is difficult to objectively reflect the behavior characteristics of autonomous vehicles on the actual road through the assumption of the operating characteristics of autonomous vehicles, such as the fact that autonomous vehicles can maintain a smaller headspace, and a shorter starting and accelerating time. Among the existing self-driving vehicle-following models, the ACC automatic driving following model proposed by the PATH Laboratory of the University of California, Berkeley, is the most widely used. This model is determined by real vehicle data, and a large number of experiments are conducted in order to calibrate model parameters, which has a certain authenticity. Therefore, the ACC autonomous vehicle-following model proposed by the PATH laboratory is selected in this paper [32], and its specific form is shown in Formulas (12) and (13).

$$a_n(t) = k_1 e_n(t) + k_2 \Delta v_n(t), \tag{12}$$

$$e_n(t) = h_n(t) - l - s_0 - t_a v_n(t), \tag{13}$$

where $a_n(t)$ represents the acceleration of the vehicle, $e_n(t)$ represents the error between actual vehicle spacing and expected vehicle spacing at the time, $\Delta v_n(t)$ represents the

difference in vehicle speed before and after the time, k_1 represents the control coefficient of workshop distance error, k_2 represents the speed difference control coefficient; $h_n(t)$ represents the space headway of the vehicle at the moment, l represents vehicle length, s_0 represents minimum expected (safety) workshop distance, t_a represents the expected time headway, and $v_n(t)$ represents speed of the vehicle at the time.

With reference to the recommended values of model parameters from the PATH laboratory, and in order to maintain the consistency of the performance of human-driven vehicles and self-driving vehicles, the values of the ACC self-driving vehicle-following model parameters, are shown in Table 2.

Table 2. Values of the ACC following model parameters.

Parameter	Value
a	1
v_0	34
s_0	1.5
b	2
l	5
t_a	1.1

2.5.3. The CACC Following Model

The second type is the autonomous vehicle based on collaborative adaptive cruise control. On the basis of the ACC autonomous vehicle, vehicle-vehicle communication is added in order to enable it to acquire the speed, acceleration, and other parameters of other vehicles around the vehicle, more quickly and accurately, further shortening the reaction time.

Similarly, since there are few real studies on existing CACC self-driving vehicles, the following model of CACC self-driving vehicles, proposed by the PATH laboratory, is also selected for this paper. For specific forms, see Formulas (14) and (15).

$$a_n(t) = k_0 a_{n-1}(t) + k_1 e_n(t) + k_2 \Delta v_n(t), \tag{14}$$

$$e_n(t) = h_n(t) - l - s_0 - t_a v_n(t), \tag{15}$$

where $a_n(t)$ represents the acceleration of the vehicle, $e_n(t)$ represents the error between actual vehicle spacing and expected vehicle spacing at the time, $\Delta v_n(t)$ represents the difference of vehicle speed before and after the time, k_0 represents the acceleration control coefficient; k_1 represents the control coefficient of workshop distance error; k_2 represents the speed difference control coefficient; $h_n(t)$ represents the space headway of the vehicle at the moment, l represents vehicle length, s_0 represents the minimum expected (safety) workshop distance, t_a represents the expected time headway, and $v_n(t)$ represents the speed of the vehicle at the time.

In the same way as the ACC model parameter values, the CACC autonomous vehicle-following model parameter values are shown in Table 3.

Table 3. Values of the CACC following model parameters.

Parameter	Value
a	1
v_0	34
s_0	1.5
b	2
l	5
t_a	0.6

3. The Homogeneous Road Traffic Flow-Density Relationship

3.1. Theoretical Derivation

Based on the basic diagram model of traffic flow, the equilibrium "speed-time headway" function relationship of traffic flow, and the vehicle-following model, the flow-density relationship of homogeneous traffic flow of different vehicle types in a single environment, can be deduced.

When the traffic flow is in an equilibrium state, the speed of all vehicles on the road is consistent, the speed difference between all vehicles is 0, and the speed of all vehicles is 0, as shown in Equation (16).

$$\begin{cases} v_n(t) = v_b \\ \Delta v = 0 \\ a_n(t) = 0 \end{cases}, \tag{16}$$

Therefore, the relationship between the headspace of the human-driven vehicle can be deduced using Formulas (9), (10), (11) and (16), as shown in Equation (17).

$$h_{dI} = h_n = \frac{s_0 + v_b T}{\sqrt{1 - (\frac{v_b}{v_0})^4}} + l, \tag{17}$$

where: h_{dI} and h_n represent the distance between the locomotive in the balanced state; v_b represents the equilibrium state velocity, and the value range is $[1, v_0)$; v_0 represents the (expected) velocity in the free flow; s_0 represents the minimum expected (safety) workshop distance; T represents the expected (minimum) headway; and l represents the length of the vehicle.

Then, through the relationships between the three parameters of traffic flow, it can be seen that there is a reciprocal relationship between the density and the distance between the heads, and the "speed-density relation" of fully manual driven vehicles can be obtained, as shown in Equation (18).

$$K_I = \frac{1000\sqrt{1 - (\frac{v_b}{v_0})^4}}{s_0 + v_b T + l\sqrt{1 - (\frac{v_b}{v_0})^4}}, \tag{18}$$

where K_I represents lane density.

In the equilibrium state, the time headway can be obtained by comparing the headway with the vehicle speed, and then the traffic volume can be obtained, as shown in Equations (19) and (20).

$$h_{tI} = \frac{h_{dI}}{v_b}, \tag{19}$$

$$Q_I = \frac{3600}{h_{tI}}, \tag{20}$$

where h_{tI} is the headway of the artificially driven vehicle in the equilibrium state, Q_I is the traffic volume of manually driven vehicle in equilibrium state.

The above represents the three-parameter relationship of traffic flow for artificially driven vehicles. Similarly, the basic graph model relationships of ACC and CACC autonomous vehicles can be deduced, respectively, through Equations (12)–(16).

The basic map model of an ACC autonomous vehicle is as follows:

$$h_{dA} = h_n = l + s_0 + t_a v_b, \tag{21}$$

$$K_A = \frac{1000}{h_{dA}}, \tag{22}$$

$$h_{tA} = \frac{h_{dA}}{v_b}, \tag{23}$$

$$Q_A = \frac{3600}{h_{tA}}, \tag{24}$$

where h_{dA} and h_n represent the distance between the heads of ACC autonomous driving vehicles in the balanced state, v_b represents the balance state speed of ACC autonomous vehicles with a value range of $[1, v_0)$, s_0 represents the minimum expected (safety) workshop distance of ACC autonomous vehicles, t_a represents the expected (minimum) headway of ACC autonomous vehicles, l represents vehicle length, K_A represents lane density at equilibrium speed, h_{tA} represents the time headway of a balanced state, and Q_A represents the traffic volume of ACC autonomous vehicles in an equilibrium state.

The basic diagram model of the CACC autonomous vehicle is as follows.

$$h_{dC} = h_n = l + s_0 + t_c v_b, \tag{25}$$

$$K_C = \frac{1000}{h_{dC}}, \tag{26}$$

$$h_{tC} = \frac{h_{dC}}{v_b}, \tag{27}$$

$$Q_C = \frac{3600}{h_{tC}}, \tag{28}$$

where: h_{dC} and h_n represent the distance between the heads of CACC autonomous driving vehicles in the balanced state, v_b represents the balanced-state velocity of a CACC autonomous vehicle with a value range of $[1, v_0)$, s_0 represents the minimum expected (safety) workshop distance of a CACC autonomous vehicle, t_c represents the expected (minimum) headway of a CACC autonomous vehicle, l represents the length of a CACC autonomous vehicle, K_C represents the lane density of a CACC autonomous vehicle at equilibrium speed; h_{tC} represents the time headway of a CACC autonomous vehicle in the equilibrium state, and Q_C represents the traffic volume of a CACC autonomous vehicle in an equilibrium state.

According to the calculation formula of the basic traffic flow diagram model of the three vehicles, the density-flow relationship between manually driven vehicles and autonomous vehicles, can be obtained by constantly changing the vehicle's equilibrium velocity v_b (from 1 to 33 in turn), as shown in Figure 1.

As can be seen from the chart above:

(1) The black solid line in the figure represents the IDM manually driven vehicle v_f.
(2) The flow-density curve of the IDM manually driven vehicles is a quadratic function, while the flow-density curve of the ACC and the CACC autonomous vehicles, is a linear function. This is because the following model selected, is of linear structure. Different from the flow-density curve of the IDM, it only has a crowded area on the right side of the diagram. By extending the intersection of the black solid line with the maximum flow point of the ACC and the CACC, the uncrowded areas of the ACC and the CACC flow density maps, can be obtained.
(3) In the flow-density diagram, the maximum flow can be approximated as road capacity, or basic saturated flow rate.
(4) When the road is full of ACC vehicles, its theoretical maximum capacity is 1.48 times that of manual vehicles; When the road is full of CACC vehicles, its theoretical maximum capacity is 2.42 times that of manual vehicles.
(5) Compared with ACC vehicles, CACC vehicles demonstrate greater improvement on road capacity.

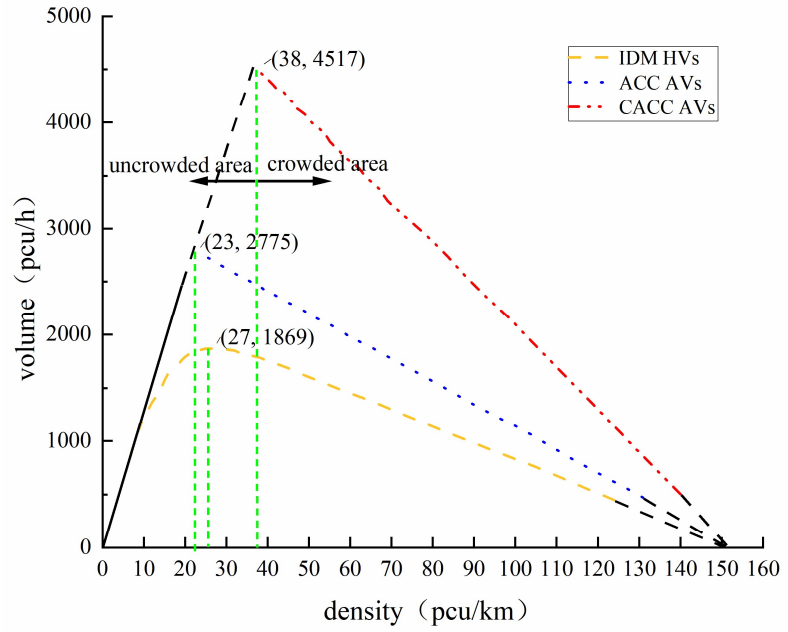

Figure 1. Flow-density diagram for a single vehicle composition.

3.2. Experimental Verification

In order to verify the correctness of the derivation of homogeneous traffic flow on a road in a single environment, SUMO was used, to build a single-lane road environment under ideal conditions, and set a balanced traffic flow for simulation. The simulation effect is shown in Figure 2. The length of the road network is 1 km, and the simulation time is 3600 s. The number of vehicles loaded is set as the maximum (10,000 in this experiment). The vehicle speed is set from 0 to v_0 and simulated successively. Since the SUMO simulation step size has a certain impact on the results, but the increase of the simulation step size will cause the exponential increase of the simulation time, this paper selected two simulation step sizes: 1 s, and 0.1 s. Table 4 shows the specific parameters of a manual vehicle, an ACC autonomous vehicle, and a CACC autonomous vehicle.

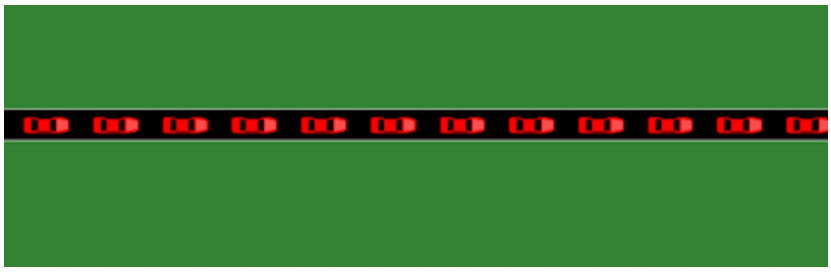

Figure 2. SUMO simulation diagram: single road traffic flow.

The data are acquired by the detector, and then processed. The flow-density relationship of three kinds of vehicles, under different simulation steps, is shown in Figure 3.

As can be seen from the figure above, as the simulation step length of SUMO becomes shorter, the simulation traffic volume keeps approaching the theoretical traffic volume. This is because the shorter the simulation step size is, the higher the simulation accuracy will be. Therefore, when the simulation step size is 1 s, there is a large error, and the average error is shown in Table 5. However, as the SUMO simulation step length becomes shorter, its simulation time increases exponentially. In order to balance the relationship between simulation error and simulation time, the simulation step size of 0.1 s is used for subsequent experiments.

Table 4. Vehicle parameter settings in SUMO.

Vehicle Type	Parameter Name	Parameter Value
manual vehicle	color	green
	carFollowModel	IDM
	length	5
	accel	1
	decel	2
	minGap	1.5
	tau	1.5
	maxSpeed	$[1, v_0)$
	delat	0
ACC autonomous vehicle	color	red
	carFollowModel	ACC
	length	5
	accel	1
	decel	2
	minGap	1.5
	tau	1.1
	maxSpeed	$[1, v_0)$
	speedDev	0
CACC autonomous vehicle	color	red
	carFollowModel	CACC
	length	5
	accel	1
	decel	2
	minGap	1.5
	tau	0.6
	maxSpeed	$[1, v_0)$
	speedDev	0

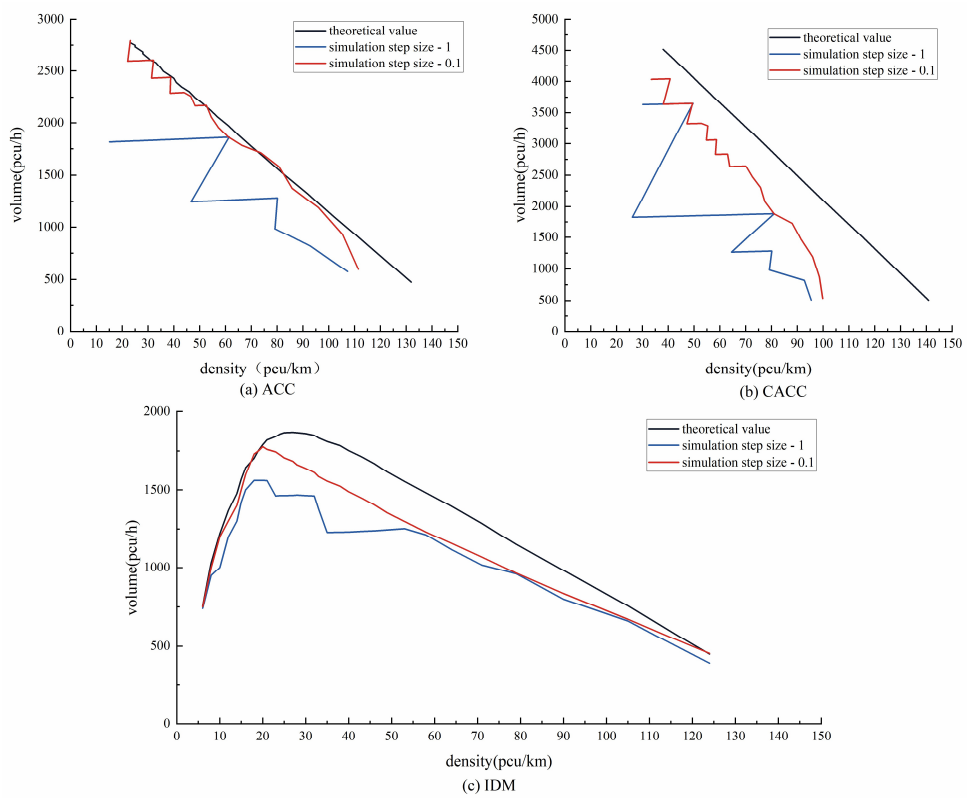

Figure 3. Flow-density graphs of different types of vehicles, based on SUMO simulation.

Table 5. The average error of actual value and theoretical value, under different simulation step sizes.

Type	Theoretical Mean	Actual Mean Value (Simulation Step Size)		Mean Absolute Error (pcu) 1–0.1 s	Mean Relative Error (%) 1–0.1 s
		1 s	0.1 s		
IDM	1526	1236	1381	290–145	19–9.5
ACC	2209	1666	2184	543–25	24.6–1.1
CACC	3314	2474	2988	840–326	25.3–9.8

By comparing fully human-driven vehicles, fully ACC autonomous vehicles, and fully CACC autonomous vehicles, it can be found that road traffic capacity is constantly increasing in theory and simulation experiments. In the simulation experiment, the maximum flow of a fully ACC autonomous driving vehicle, is 1.48 times that of a fully manual driving vehicle. The maximum flow rate of a fully CACC autonomous vehicle is 2.14 times that of a fully manual vehicle, which is close to the theoretical value. This proves that the model is correct.

4. The Road Heterogeneous Traffic Flow Flow-Density Relationship

At present, there are two kinds of autonomous vehicles: ACC autonomous vehicles, and CACC autonomous vehicles. If the CACC vehicle in front of it is an ACC vehicle, or the human-driven vehicle does not have a communication module, then the CACC vehicle automatically degenerates into an ACC vehicle. As such, there are three possible mixing conditions on the road:

(1) HVs and ACC AVs;
(2) HVs, ACC AVs and CACC AVs;
(3) HVs and CACC AVs.

Despite the continuous development of vehicle technology, ACC autonomous driving vehicles in the man-machine hybrid driving environment on the road are only at the transition stage, though eventually road vehicles will mainly consist of human-driven vehicles and CACC autonomous driving vehicles. Therefore, this paper does not consider the mixing of ACC vehicles separately, and the man-machine hybrid driving environment only targets the third situation. That is, all autonomous vehicles are considered to be CACC autonomous vehicles.

4.1. Derivation of the Proportions of All Types of Vehicles

When the vehicles in the mixed environment are composed only of human-driven vehicles and CACC vehicles, there are only six cases of vehicle distribution, as shown in Figure 4.

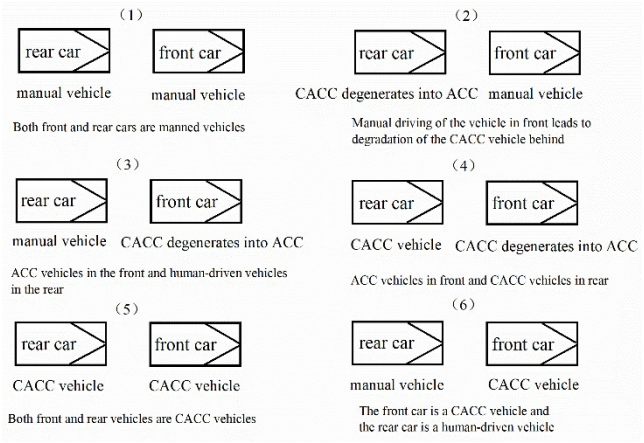

Figure 4. Distribution of vehicles in a mixed environment.

Assuming that the total number of vehicles on the road is n and that the proportion of CACC vehicles is set as $p(0 \leq p \leq 1)$ then the proportion of manually driven vehicles is $1-p$. When the vehicle in front of the CACC autonomous vehicle is a human-driven vehicle, the front and rear vehicles cannot communicate with each other, so the CACC vehicle automatically changes into ACC following mode, and thus becomes an ACC autonomous vehicle. Based on probability theory, the expected proportion of ACC autonomous vehicles on the road can be calculated as $(1-p)p$, such that the actual number of CACC vehicles on the road is calculated as $np - n(1-p)p = np^2$.

The following proportion formula can be obtained:

$$p_c = p^2, \tag{29}$$

$$p_a = p(1-p), \tag{30}$$

$$p_i = 1-p, \tag{31}$$

and the proportional relationship satisfies the following constraints.

$$\begin{cases} p_c + p_a + p_i = 1 \\ p_c + p_a = p \\ p_a \leq p_i \\ p_a \leq p \end{cases}, \tag{32}$$

where: p denotes the blending rate of CACC autonomous vehicles, p_c represents the actual mixing rate of CACC vehicles on the road, p_a represents the blending rate of ACC vehicles on actual roads, and p_i represents the blending rate of actual road artificially-driven vehicles.

4.2. Derivation of Flow-Density Theory

Through the analysis of IDM, CACC, and ACC following models, it can be seen that, in this case, when the traffic flow reaches the equilibrium state, all vehicles have the same speed, but different vehicles have different space headway, as shown in Figure 5. Suppose that the road length is L. In that case, h_{dI}, h_{dA}, and h_{dC} are the three respective space headways maintained by the three types of vehicles in the equilibrium state.

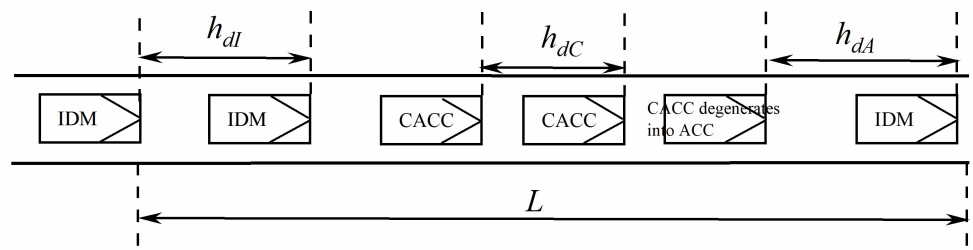

Figure 5. Balance in a man-machine hybrid driving environment.

In the equilibrium state, the road length covered by the traffic flow composed of different vehicle types, is shown in Equation (33).

$$L = np_c h_{dC} + np_a h_{dA} + np_i h_{dI} \tag{33}$$

According to the calculation formula of traffic flow density, the function of equilibrium speed-front spacing, and the formula derived from the proportion of various vehicles, the basic density-speed graph relationship can be obtained, as follows:

$$K = \frac{n}{L} = \frac{1000}{p_c h_{dC} + p_a h_{dA} + p_i h_{dI}}, \tag{34}$$

$$h_t = \frac{(1-p)h_{dI} + p(1-p)h_{dA} + p^2 h_{dC}}{v_b}, \tag{35}$$

$$Q = \frac{3600}{h_t}, \tag{36}$$

where K is lane density in mixed environment, h_t is the headway in mixed environment, Q is the traffic volume in a mixed environment.

According to the flow-density relationship of the traffic flow of mixed vehicles, the density-flow diagram of the mixed vehicles can be obtained by constantly changing the balance speed (v_b) of the vehicles, and the proportion of autonomous vehicles. This is demonstrated in Figure 6, where p represents the proportion of CACC autonomous vehicles in the total road vehicles.

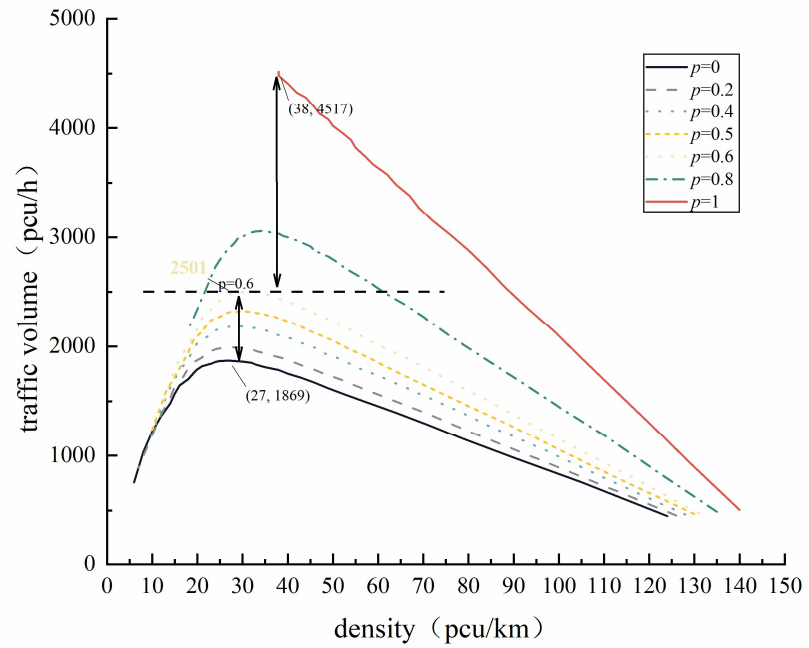

Figure 6. Flow-density diagram in a mixed environment with different autopilot proportions.

As can be seen from the chart above:

(1) For single-lane roads, the increase in the proportion of autonomous vehicles, contributes to the improvement of road traffic capacity. Moreover, when a road contains only autonomous vehicles, its traffic capacity is 2.42 times that of the traffic capacity of a road containing only fully human-driven vehicles.

(2) The dividing line for the proportion of self-driving vehicles in the total road vehicles, is 0.6. When the proportion is below 0.6, then mixing of self-driving vehicles can improve the road traffic capacity, although the overall improvement is small; When the ratio is above 0.6, then the inclusion of autonomous vehicles greatly improves the road traffic capacity. The increase of the ratio above 0.6 was 3.19 times that of the ratio below 0.6.

4.3. Experimental Verification

In order to verify the correctness of the derivation of the single-lane heterogeneous traffic flow theory, a single-lane road in a mixed environment was established by SUMO, and then simulated. The simulation operation was shown in Figure 7, in which the human-driven vehicle was colored green, and the autonomous vehicle was colored red.

The simulation step is 0.1 s, and other simulation conditions are consistent with those in Section 3. The balance speed, v_b, of hybrid vehicles, is set successively from $0 - v_0$, and the vehicle flow is counted by a detector arranged at the road's starting point.

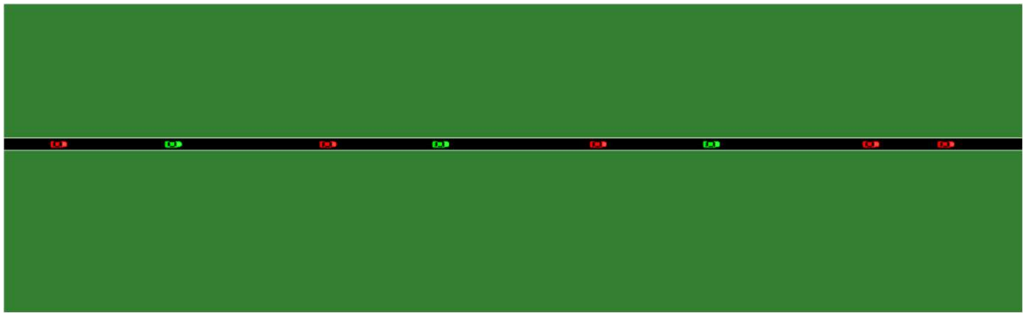

Figure 7. SUMO simulation diagram: traffic flow in a mixed environment.

In the case of different proportions of autonomous vehicles, the average error between the theoretical value and the actual value, is shown in Table 6.

Table 6. Average errors of actual and theoretical traffic volumes under different proportions of autonomous vehicles.

The Proportion of Autonomous Driving	Theoretical Mean	Actual Mean	Mean Absolute Error (pcu)	Mean Relative Error (%)
0	1526	1381	145	9.5
0.1	1574	1508	66	4.2
0.2	1632	1529	103	6.3
0.3	1704	1559	145	8.5
0.4	1794	1584	210	11.7
0.5	1905	1609	296	15.5
0.6	2047	1756	291	14.2
0.7	2229	1942	287	12.9
0.8	2470	2171	299	12.1
0.9	2806	2493	313	11.2
1.0	3313	2988	325	9.8

As can be seen from the above table, the relative error between the theoretical average and the actual average of the traffic volume of autonomous vehicles with different proportions is no more than 16%, indicating that the deduced flow-density relation of heterogeneous traffic flow on the road is correct.

5. Capacity Calculation Model of Signalized Intersection in a Mixed Environment

5.1. Capacity Calculation Model of Signalized Intersection

Through the analysis of the previous sections, it can be seen that the calculation of capacity at signalized intersections is mostly calculated by saturated flow rate (or saturated flow rate), and the saturated flow rate is modified on the basis of the basic saturated flow rate, which is the maximum traffic volume passing through a certain section of the road in a certain unit of time. Based on the derivation of the flow-density of road homogeneous traffic flow in this chapter, the basic saturated flow rate of a road under a man-machine hybrid driving environment, can be easily obtained.

Therefore, this section proposes using a revised calculation model for assessing signalized intersection capacity in a mixed environment, which can essentially be used to identify the basic saturated flow rate in a mixed environment, as shown in Table 7.

Table 7. Basic saturated flow rate of single lane under different automatic driving proportions.

The Proportion of Autonomous Driving	Basic Saturation Flow Rate (pcu/h)
0.0	1869
0.1	1923
0.2	1991
0.3	2077
0.4	2186
0.5	2324
0.6	2501
0.7	2735
0.8	3054
0.9	3527
1.0	4517

5.2. Case Analysis

In order to verify the accuracy of the proposed calculation model of capacity correction for signalized intersections in a mixed environment, SUMO was used, to design simulation experiments involving different proportions of autonomous vehicles in different CACCs, with the number of vehicles passing the stop line in each lane counted, for purposes of comparison with the theoretical conversion results.

The simulation section represents a standard intersection, with a lane width of 3.0 m. The simulation operation is shown in Figure 8. The detector is placed on the stop line, the red vehicle is an automatic vehicle, and the green vehicle is a manual vehicle. The traditional four-phase timing scheme is adopted, and the signal cycle is 120 s. Figure 9 shows the green time of each phase, wherein the yellow time is 3 s, the vehicle speed is 33 m/s, and the number of vehicles is the largest. The vehicle parameters are shown in Table 4. The simulation duration is 3600 s, the simulation step is 0.1 s, and the right-turn lane is ignored.

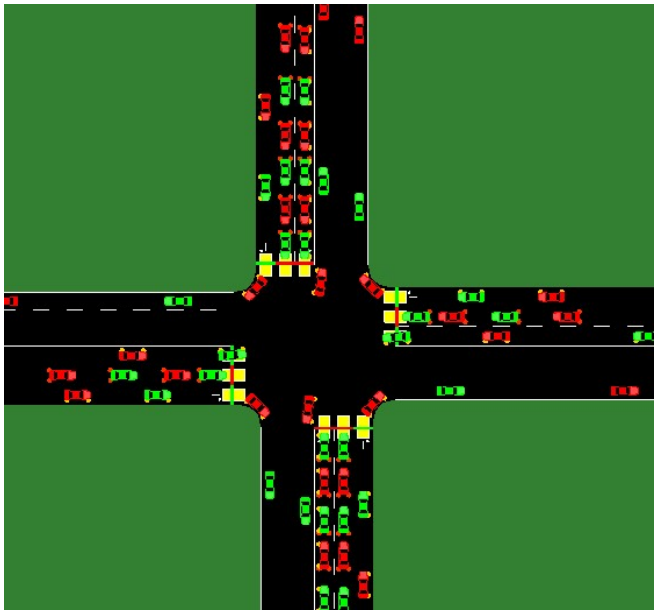

Figure 8. SUMO simulation diagram: intersection capacity in a mixed environment.

Risk factor assessment and mitigation measures:

(1) Using a large range of road networks will increase the simulation time and calculation amount, resulting in inaccurate simulation results. In this paper, the standard signal control intersection was selected in the experimental verification stage.

(2) The type and number of lanes at the intersection also impact the experiment. To this end, independent lanes were selected for each entrance direction of the intersection.

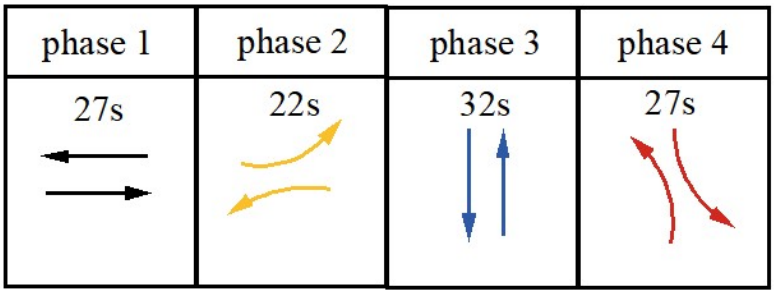

Figure 9. Signal timing scheme.

The capacity of signalized intersections in a mixed environment is calculated according to Table 7 and Equations (1)–(3). The conversion coefficient is shown in Table 8.

Table 8. Modified parameter values.

Parameter Name	Number of Lanes	Lane Width	Load Rate and Slope	Green Signal Ratio
value	1	1	0.95	0.2

Take the east entrance straight lane as an example: the capacity of the lane converted by theory is compared with the actual traffic volume simulated by SUMO, as shown in Figure 10. The relative error is less than 16%, which proves that the deduced capacity of the signalized intersection in the mixed environment is more in line with the actual situation. In addition, with the increase of the proportion of autonomous vehicles, the capacity of the intersection is also increasing. When the intersection is full of AVs, its capacity is 2.40 times that of fully HVs.

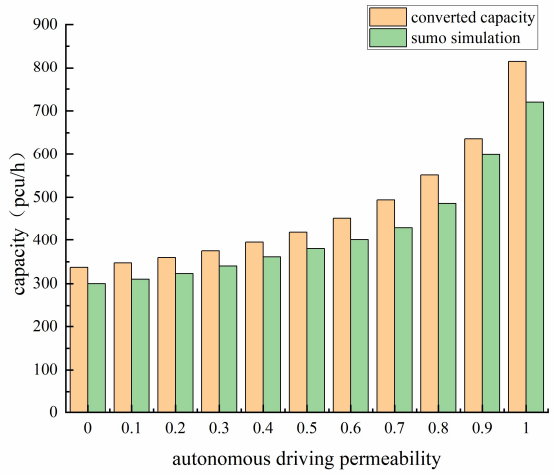

Figure 10. Capacity of the straight lane at the east entrance of the intersection.

6. Conclusions and Future Work

A revised model of intersection capacity calculation, based on saturated flow rate, is proposed in a mixed environment, which is essentially the calibration of the basic saturated flow rates under different automatic driving proportions. Firstly, the flow density relationship of different types of vehicles on a single lane road is proposed, using the basic traffic flow diagram model, traffic flow equilibrium analysis, and the vehicle-following model. Then, the flow density relationship of heterogeneous traffic flows in a single lane is obtained according to the proportional derivation of various vehicles. The results show

that autonomous vehicles can greatly improve road traffic efficiency. When ACC vehicles are all on the road, their maximum traffic capacity is 1.48 times that of artificial vehicles. When the road is full of CACC vehicles, its maximum capacity is 2.42 times that of manual vehicles. As the proportion of autonomous vehicles increases, so too does road capacity; based on the calculation formula of signalized intersection capacity, the calculation model of intersection capacity under a mixed environment, is obtained. The results show that the mixing of automatic driving and human driving will improve the intersection capacity, but the improvement degree is small, mainly affected by intersection signal control. The three cases are verified by SUMO simulation.

The essence of the calculation of the capacity of a signalized intersection in a man-machine hybrid driving environment proposed in this paper, is to calibrate the basic saturated flow rate under different proportions of autonomous vehicles, and then calculate it through the method in HCM. However, with the development of artificial intelligence, big data, and other technologies, the research on intersection capacity can also be obtained through traffic flow prediction [33–35]. Therefore, the authors of this paper will study the following in the future:

(1) The capacity of roads and intersections in a human-machine mixed environment will be studied by means of the methods related to traffic flow prediction;
(2) To study the impact of autonomous vehicles on road traffic flow by means of machine learning;
(3) The capacity of roads and intersections obtained by the new method will be compared with that obtained by the traditional method.

Author Contributions: Conceptualization, Q.Y. and H.Z.; Data curation, H.Z.; Formal analysis, Q.Y.; Investigation, Q.Y.; Methodology, H.Z.; Project administration, Q.Y.; Resources, Q.Y.; Software, L.W. (Long Wu); Supervision, L.L.; Validation, L.L. and L.W. (Li Wang); Visualization, L.W. (Long Wu); Writing—original draft, H.Z.; Writing—review and editing, H.Z. All authors have read and agreed to the published version of the manuscript.

Funding: This research received no external funding.

Institutional Review Board Statement: Not applicable.

Informed Consent Statement: Not applicable.

Data Availability Statement: The data presented in this study are available upon request from the corresponding author.

Acknowledgments: The authors would like to sincerely thank all of the people who assisted them in completing this paper.

Conflicts of Interest: The authors declare no conflict of interest.

References

1. Ahmed, H.U.; Huang, Y.; Lu, P.; Bridgelall, R. Technology developments and impacts of connected and autonomous vehicles: An overview. *Smart Cities* **2022**, *5*, 382–404. [CrossRef]
2. Park, J.E.; Byun, W.; Kim, Y.; Ahn, H.; Shin, D.K. The impact of automated vehicles on traffic flow and road capacity on urban road networks. *J. Adv. Transp.* **2021**, *2021*, 8404951. [CrossRef]
3. Beza, A.D.; Maghrour Zefreh, M.; Torok, A. Impacts of different types of automated vehicles on traffic flow characteristics and emissions: A microscopic traffic simulation of different freeway segments. *Energies* **2022**, *15*, 6669. [CrossRef]
4. Song, H.; Zhao, F.; Liu, Z. Influences of single-lane automatic driving systems on traffic efficiency and CO_2 emissions on China's motorways. *Appl. Sci.* **2021**, *11*, 11032. [CrossRef]
5. Lu, Q.; Tettamanti, T.; Hörcher, D.; Varga, I. The impact of autonomous vehicles on urban traffic network capacity: An experimental analysis by microscopic traffic simulation. *Transp. Lett.* **2020**, *12*, 540–549. [CrossRef]
6. Mavromatis, I.; Tassi, A.; Piechocki, R.J.; Sooriyabandara, M. On urban traffic flow benefits of connected and automated vehicles. In Proceedings of the IEEE 91st Vehicular Technology Conference (VTC2020-Spring), Antwerp, Belgium, 25–28 May 2020; Volume 2020, pp. 1–7.
7. Ghiasi, A.; Hussain, O.; Qian, Z.S.; Li, X. A mixed traffic capacity analysis and lane management model for connected automated vehicles: A Markov chain method. *Transp. Res. Part B Methodol.* **2014**, *106*, 266–292. [CrossRef]

8. Van Arem, B.; Van Driel, C.J.; Visser, R. The impact of cooperative adaptive cruise control on traffic-flow characteristics. *IEEE Trans. Intell. Transp. Syst.* **2006**, *7*, 429–436. [CrossRef]
9. VanderWerf, J.; Shladover, S.; Miller, M.A. *Conceptual Development and Performance Assessment for the Deployment Staging of Advanced Vehicle Control and Safety Systems*; University of California: Berkeley, CA, USA, 2004.
10. Kesting, A.; Treiber, M.; Schönhof, M.; Kranke, F.; Helbing, D. Jam-avoiding adaptive cruise control (ACC) and its impact on traffic dynamics. In *Traffic and Granular Flow'05*; Springer: Berlin/Heidelberg, Germany, 2007; pp. 633–643.
11. Shladover, S.E.; Su, D.; Lu, X.Y. Impacts of cooperative adaptive cruise control on freeway traffic flow. *Transp. Res. Rec.* **2012**, *2324*, 63–70. [CrossRef]
12. Li, X.; Xiao, Y.; Zhao, X.; Ma, X.; Wang, X. Modeling mixed traffic flows of human-driving vehicles and connected and autonomous vehicles considering human drivers' cognitive characteristics and driving behavior interaction. *Phys. A Stat. Mech. Its Appl.* **2023**, *609*, 128368. [CrossRef]
13. Vander Werf, J.; Shladover, S.E.; Miller, M.A.; Kourjanskaia, N. Effects of adaptive cruise control systems on highway traffic flow capacity. *Transp. Res. Rec.* **2002**, *1800*, 78–84. [CrossRef]
14. Jones, S.; Philips, B.H. Cooperative adaptive cruise control: Critical human factors issues and research questions. In Proceedings of the Driving Assesment Conference, Bolton Landing, NY, USA, 17–20 June 2013; University of Iowa: Iowa City, IA, USA, 2013; Volume 7.
15. Calvert, S.C.; Schakel, W.J.; Van Lint, J.W.C. Will automated vehicles negatively impact traffic flow? *J. Adv. Transp.* **2017**, *2017*, 3082781. [CrossRef]
16. Tientrakool, P.; Ho, Y.C.; Maxemchuk, N.F. Highway capacity benefits from using vehicle-to-vehicle communication and sensors for collision avoidance. In Proceedings of the 2011 IEEE Vehicular Technology Conference (VTC Fall), San Francisco, CA, USA, 5–8 September 2011; Volume 2011, pp. 1–5.
17. Ko, Y.; Rho, J.H.; Donghyung, Y. Assessing benefits of autonomous vehicle system implementation through the network capacity analysis. *Korea Spat. Plan. Rev.* **2017**, *93*, 17–24.
18. Meyer, J.; Becker, H.; Bösch, P.M.; Axhausen, K.W. Autonomous vehicles: The next jump in accessibilities? *Res. Transp. Econ.* **2017**, *62*, 80–91. [CrossRef]
19. Kang, M.H.; Lm, I.J.; Song, J.I.; Hwang, K.Y. Analyzing Traffic Impacts of Auto-mated Vehicles on Expressway Weaving Sections. *J. Transp. Res.* **2019**, *26*, 33–47.
20. Arnaout, G.M.; Arnaout, J.P. Exploring the effects of cooperative adaptive cruise control on highway traffic flow using microscopic traffic simulation. *Transp. Plan. Technol.* **2014**, *37*, 186–199. [CrossRef]
21. Liu, H.; Kan, X.D.; Shladover, S.E.; Lu, X.Y.; Ferlis, R.E. Modeling impacts of cooperative adaptive cruise control on mixed traffic flow in multi-lane freeway facilities. *Transp. Res. Part C Emerg. Technol.* **2018**, *95*, 261–279. [CrossRef]
22. Yu, S.; Shi, Z. The effects of vehicular gap changes with memory on traffic flow in cooperative adaptive cruise control strategy. *Phys. A Stat. Mech. Its Appl.* **2015**, *428*, 206–223. [CrossRef]
23. Atkins, W.S. Research on the impacts of connected and autonomous vehicles (CAVs) on traffic flow. In *Stage 2: Traffic Modelling and Analysis Technical Report*; Department for Transport: London, UK, 2016.
24. Li, D.; Wagner, P. Impacts of gradual automated vehicle penetration on motorway operation: A comprehensive evaluation. *Eur. Transp. Res. Rev.* **2019**, *11*, 36. [CrossRef]
25. Ko, W.; Park, S.; So, J.J.; Yun, I. Analysis of effects of autonomous vehicle market share changes on expressway traffic flow using IDM. *J. Korea Inst. Intell. Transp. Syst.* **2021**, *20*, 13–27. [CrossRef]
26. Kittelson, W.K.; Roess, R.P. Highway capacity analysis after highway capacity manual 2000. *Transp. Res. Rec.* **2001**, *1776*, 10–16. [CrossRef]
27. Roess, R.P.; Prassas, E.S. *The Highway Capacity Manual: A Conceptual and Research History*; Springer: Cham, Switzerland, 2014.
28. Allsop, R.E. Estimating the traffic capacity of a signalized road junction. *Transp. Res.* **1972**, *6*, 245–255. [CrossRef]
29. Yagar, S. Capacity of a signalized road junction: Critique and extensions. *Transp. Res.* **1974**, *8*, 137–147. [CrossRef]
30. Greenshields, B.D.; Bibbins, J.R.; Channing, W.S.; Miller, H.H. A study of traffic capacity. *Highw. Res. Board Proc.* **1935**, *14*, 448–477.
31. Treiber, M.; Hennecke, A.; Helbing, D. Congested traffic states in empirical observations and microscopic simulations. *Phys. Rev. E* **2000**, *62*, 1805. [CrossRef]
32. Milanés, V.; Shladover, S.E. Modeling cooperative and autonomous adaptive cruise control dynamic responses using experimental data. *Transp. Res. Part C Emerg. Technol.* **2014**, *48*, 285–300. [CrossRef]
33. Shah, I.; Muhammad, I.; Ali, S.; Ahmed, S.; Almazah, M.M.A.; Al-Rezami, A.Y. Forecasting Day-Ahead Traffic Flow Using Functional Time Series Approach. *Mathematics* **2022**, *10*, 4279. [CrossRef]
34. Peng, H.; Wang, H.; Du, B.; Bhuiyan, M.Z.A.; Ma, H.; Liu, J.; Philip, S.Y. Spatial temporal incidence dynamic graph neural networks for traffic flow forecasting. *Inf. Sci.* **2020**, *521*, 277–290. [CrossRef]
35. Rastgoo, M.N.; Nakisa, B.; Maire, F.; Rakotonirainy, A.; Chandran, V. Automatic driver stress level classification using multimodal deep learning. *Expert Syst. Appl.* **2019**, *138*, 112793. [CrossRef]